ARTICLE

Open Access

First observation of tropospheric nitrogen dioxide from the Environmental Trace Gases Monitoring Instrument onboard the GaoFen-5 satellite

Chengxin Zhang [1], Cheng Liu[2,3,4,5], Ka Lok Chan[6], Qihou Hu[3], Haoran Liu[1], Bo Li[1], Chengzhi Xing[1], Wei Tan[3], Haijin Zhou[3], Fuqi Si[3] and Jianguo Liu[3,4]

Abstract

The Environmental Trace Gases Monitoring Instrument (EMI) is the first Chinese satellite-borne UV–Vis spectrometer aiming to measure the distribution of atmospheric trace gases on a global scale. The EMI instrument onboard the GaoFen-5 satellite was launched on 9 May 2018. In this paper, we present the tropospheric nitrogen dioxide (NO_2) vertical column density (VCD) retrieval algorithm dedicated to EMI measurement. We report the first successful retrieval of tropospheric NO_2 VCD from the EMI instrument. Our retrieval improved the original EMI NO_2 prototype algorithm by modifying the settings of the spectral fit and air mass factor calculations to account for the on-orbit instrumental performance changes. The retrieved EMI NO_2 VCDs generally show good spatiotemporal agreement with the satellite-borne Ozone Monitoring Instrument and TROPOspheric Monitoring Instrument (correlation coefficient R of ~0.9, bias < 50%). A comparison with ground-based MAX-DOAS (Multi-Axis Differential Optical Absorption Spectroscopy) observations also shows good correlation with an R of 0.82. The results indicate that the EMI NO_2 retrieval algorithm derives reliable and precise results, and this algorithm can feasibly produce stable operational products that can contribute to global air pollution monitoring.

Introduction

The Environmental Trace Gases Monitoring Instrument (EMI)[1] is the first Chinese satellite-borne spectrometer with the aim to measure atmospheric pollutants from space. The EMI payload onboard the GaoFen-5 satellite was successfully launched on 9 May 2018. The GaoFen-5 satellite has a polar orbit at an altitude of 706 km. The Chinese EMI instrument is expected to contribute to the understanding of global air quality and atmospheric chemistry, similar to predecessor European and American satellite missions, e.g., the Ozone Monitoring Instrument

(OMI)[2] and TROPOspheric Monitoring Instrument (TROPOMI)[3]. EMI has instrumental characteristics that are similar to OMI and TROPOMI, e.g., the local overpass time at ~13:30, spectral coverage, push-broom imaging technique, and daily global coverage. Both EMI and TROPOMI (launched in 2017) are new-generation satellite-borne air pollutant sensors compared to the OMI that was launched in 2004. TROPOMI follows the heritage of OMI in both instrument design and trace gas retrievals, but with higher spatial resolution and signal-to-noise ratio. A prototype EMI nitrogen dioxide (NO_2) retrieval algorithm was developed before launch based on the OMI NO_2 retrieval. However, optimization of the NO_2 retrieval algorithm was necessary to adapt the unexpected issues of EMI after launch, especially spectral calibration.

Nitrogen oxides (NO_x), defined as the sum of nitrogen oxide and NO_2, are the major pollutants contributing to ozone and secondary aerosol formation in the

Correspondence: Cheng Liu (chliu81@ustc.edu.cn) or Ka Lok Chan (ka.chan@dlr.de)
[1]School of Earth and Space Sciences, University of Science and Technology of China, Hefei 230026, China
[2]Department of Precision Machinery and Precision Instrumentation, University of Science and Technology of China, Hefei 230026, China
Full list of author information is available at the end of the article
These authors contributed equally: Chengxin Zhang, Cheng Liu

troposphere through photochemical reactions[4]. Sources of NO_x include fossil fuel combustion, vehicle emissions, biomass burning, and lightning[5]. Due to rapid industrialization and urbanization in the past few decades, China has become one of the largest NO_x emitters in the world[6]. As a result, China is experiencing a series of severe air pollution problems[7,8]. In addition to measuring NO_2 distribution directly from space, applications of satellite remote sensing may include estimations of pollutant emissions[9], air quality trend detection[10], model validation, and assimilation of satellite data[11].

Figure 1a illustrates the optical design of the EMI satellite instrument. The EMI instrument covers the ultraviolet (UV) and visible (Vis) spectral ranges from 240 to 710 nm with a spectral resolution of 0.3–0.5 nm. Light received by the telescope is depolarized by a scrambler and subsequently split into four spectral channels, the UV1 (240–315 nm), UV2 (311–403 nm), VIS1 (401–550 nm), and VIS2 (545–710 nm) channels. Each spectrometer is equipped with a two-dimensional charge-coupled device (CCD) detector, with one dimension used for spectral coverage and the other dimension used for spatial coverage. The EMI instrument scans in the nadir direction toward the earth's surface with an opening angle of 114° corresponding to a swath width of 2600 km, enabling daily global coverage with a nadir resolution of $12 \times 13 \, km^2$ and a local overpass time of 13:30 (Fig. 1b). The direct sun solar irradiance spectrum, typically used as a reference spectrum in the spectral analysis of the nadir radiance measurement, is introduced to the EMI telescope once a day using the quartz volume diffuser[12]. By using the unique absorption features of different trace gases in the UV–Vis range, the abundances of atmospheric pollutants can be retrieved from the difference between atmospheric and solar spectra.

In this paper, we present a new tropospheric NO_2 vertical column density (VCD, i.e., the vertical integral of NO_2 concentration from the earth's surface to the top of the atmosphere) retrieval algorithm dedicated to the EMI instrument. Details of the spectral retrieval, stratospheric–tropospheric separation of the NO_2 column and slant to vertical column conversion are presented. The first EMI retrieval of tropospheric NO_2 columns is compared to datasets from modern state-of-the-art European and American satellite sensors.

Results
NO_2 retrieval overview

The retrieval of tropospheric NO_2 VCDs from satellite UV–Vis observations typically follows a state-of-the-art three-step approach. First, the total NO_2 slant column density (SCD) are retrieved from nadir radiance spectra normalized by the solar irradiance, using the differential optical absorption spectroscopy (DOAS) technique[13]. Subsequently, the stratospheric NO_2 columns are separated from the total NO_2 SCDs by assuming longitudinal homogeneity of stratospheric NO_2, while neglecting the minor contribution of tropospheric NO_2 (usually on the order of 10^{14} molecules cm^{-2}) over remote clean regions[14,15]. Last, tropospheric NO_2 SCDs are converted to VCDs using air mass factors (AMFs)[16]. The AMF is defined as the ratio between SCD and VCD. It is a measure of the effective optical path length from the top of the atmosphere to the earth's surface and reflected to the satellite through the atmosphere:

$$M = \frac{S}{V} \tag{1}$$

where M is the AMF, S denotes the SCD, and V represents the VCD. The AMF can be calculated with a radiative
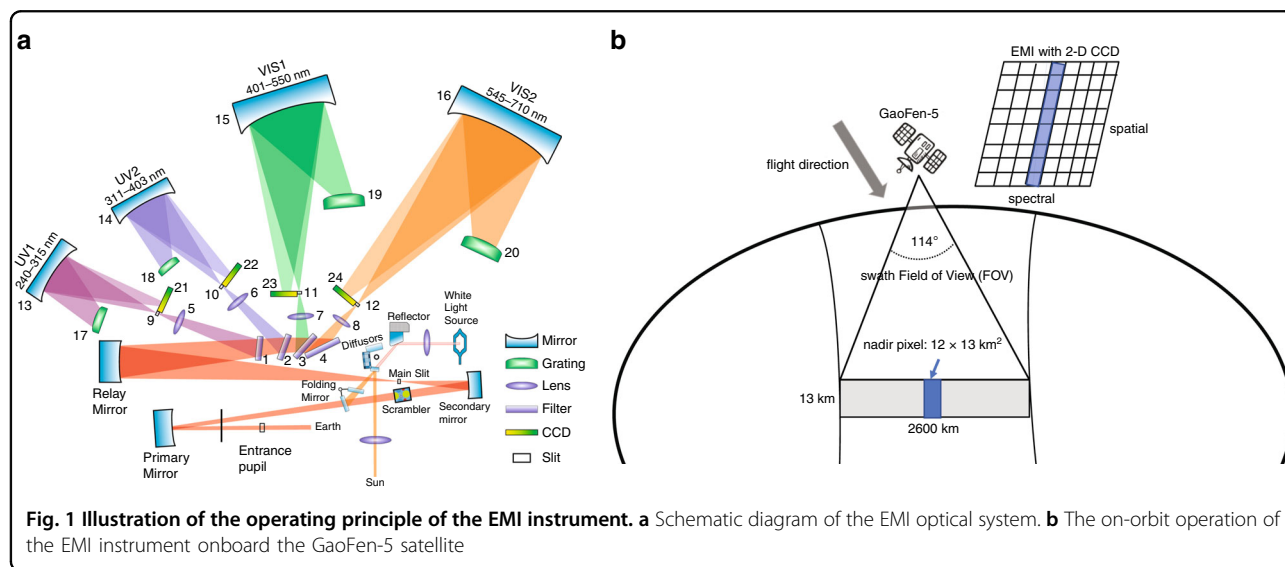

Fig. 1 Illustration of the operating principle of the EMI instrument. a Schematic diagram of the EMI optical system. **b** The on-orbit operation of the EMI instrument onboard the GaoFen-5 satellite
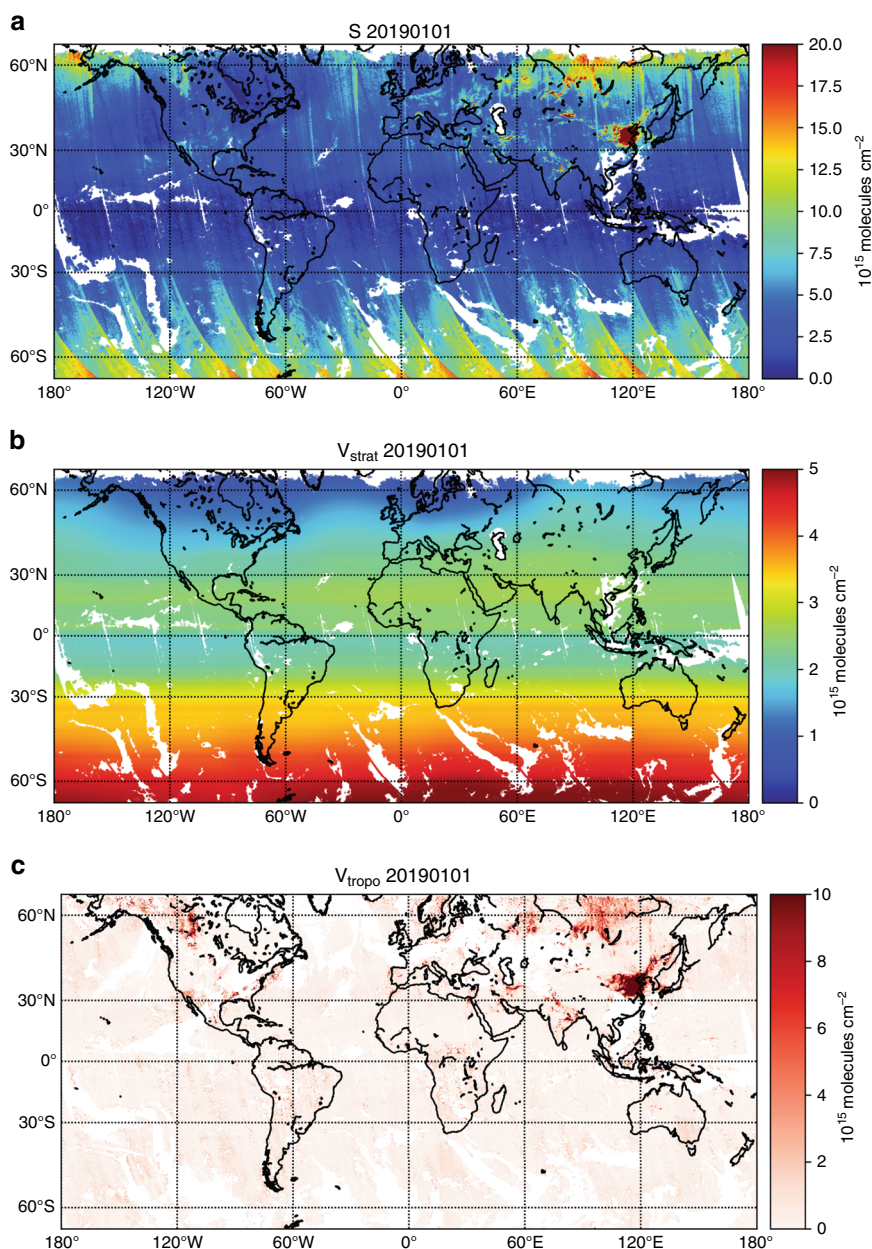
Fig. 2 An example of EMI NO$_2$ retrieval on 1 January 2019. The total SCDs (S), stratospheric VCDs (V_{strat}), and tropospheric VCDs (V_{tropo}) retrieval of NO$_2$ are shown in **a**, **b**, and **c**, respectively. Note that satellite ground pixels affected by clouds are indicated in white

transfer model (RTM). The final tropospheric NO$_2$ VCD can be derived after subtracting the stratospheric contribution and AMF conversion:

$$V_{tropo} = \frac{S - V_{strat} \times M_{strat}}{M_{tropo}} = \left(\frac{S}{M_{strat}} - V_{strat} \right) \times \frac{M_{strat}}{M_{tropo}}$$
(2)

where V_{tropo} and V_{strat} denote tropospheric and stratospheric V, respectively. M_{tropo} and M_{strat} represent

tropospheric and stratospheric M, respectively. Details of the stratospheric estimation and AMF calculation are provided in the "Materials and methods" section.

Figure 2 shows an example of EMI NO$_2$ retrieval of S, V_{strat}, and V_{tropo} on 1 January 2019. Enhanced NO$_2$ levels are observed in Eastern China, India, and the Middle East.

Algorithm improvements

A prototype EMI NO$_2$ retrieval is developed before launch. The prototype algorithm is very similar to the

Table 1 NO$_2$ retrieval settings used in the EMI and OMI NO$_2$ algorithms

Configurations and parameters	OMI NO$_2$ product (Boersma et al.[17])	EMI NO$_2$ product (in this study)
NO$_2$ SCDs fitting		
Wavelength range	405–465 nm	420–470 nm
Radiometric calibration	Using calibrated (ir)radiance[30]	Recalibrated the earth radiance measurements
Reference spectrum	Solar irradiance averaged between 2005–2009 (ref. [30])	Daily earth radiance over the remote Pacific
Instrument slit function	Preflight measured[31]	Calibrated online by using solar atlas[22], Gaussian shape assumed.
NO$_2$ AMF calculations		
Radiative transfer model (RTM)	Doubling-Adding KNMI (DAK) model[17]	Vector Linearized Discrete Ordinate Radiative Transfer (VLIDORT) model[14]
Calculation method	Lookup table interpolation	Lookup table interpolation
A priori NO$_2$ profile	The global chemistry Transport Model version 5 (TM5)[32] simulations at $1 \times 1°$	The GEOS-Chem v10-01 at $2 \times 2.5°$ for the global domain[33], and WRF-Chem v3.7 at ~20 km for the China domain[34]
Stratospheric–tropospheric separation	Data assimilation[17]	Reference sector method[14]

operational OMI NO$_2$ retrieval[17]. However, due to unexpected issues, i.e., low signal-to-noise ratio at the edges of the spectral channels, bad irradiance measurement due to a diffuser calibration issue, and spectral saturation issue, the NO$_2$ retrieval setting must be further optimized to address these issues. A series of sensitivity tests, including cloud correction, fitting wavelength range, reference selection, and spectral precalibration, have been performed to optimize the settings for tropospheric NO$_2$ VCD retrieval. Table 1 lists the updated retrieval settings of the EMI NO$_2$ retrieval. Parameters used in the OMI QA4ECV NO$_2$ retrieval[17] are also listed for reference.

The EMI NO$_2$ fitting range is shifted slightly from 405–465 nm (OMI operational NO$_2$ setting[17]) to 420–470 nm to avoid the lower signal-to-noise ratio region at the edges of the VIS1 channel[12]. Figure 3 illustrates an example of the retrieval of NO$_2$ SCD, i.e., the NO$_2$ amount integrated along the optical path in the atmosphere, by applying the DOAS fit to the EMI-measured spectrum.

The spectral saturation issue (i.e., the analogue photon signal reaches the maximum digital value of the CCD detector) is critical for EMI observations over bright clouds due to its high surface reflectance. Supplementary Figure 1 shows the global spatial pattern of the root mean square (RMS) of the spectral fitting residual, cloud radiance fraction from TROPOMI observations, and the true color image from the MODIS-Aqua instrument on 1 January 2019. The spatial pattern of the fitting residual RMS is correlated to the cloud pattern. Therefore, we filtered pixels with relatively large spectral fitting residuals, i.e., the RMS values >0.004.

The key calibration data measured during the on-ground calibration[12] seem unsuitable for EMI on-orbit measurements due to the degradation and stability of the instrument in the complex space environment (e.g., cosmic radiation exposure[18] and possible instrument changes since launch[19]). Therefore, we recalibrated the EMI earth radiance measurements by comparing the EMI radiance to TROPOMI measurements and RTM simulations. An advantage of DOAS is that it does not rely on precisely calibrated radiance and is less sensitive to the variability in radiometric calibration than other methods based on discrete radiance (e.g., SBUV and TOMS ozone retrieval algorithms[20]).

Figure 4 shows the comparisons of NO$_2$ SCDs for one orbit on 4 January 2019 retrieved using these spectral fitting scenarios: (a) current settings of the EMI NO$_2$ retrieval listed in Table 1; (b) using the measured irradiance spectrum as a reference; and (c) same as in (a) but without spectral precalibration. Irradiance spectra measured by EMI are currently accounting for some calibration issues, and these issues are probably related to the interference of the space environment on the hemispheric reflectance of solar diffusers[18]. NO$_2$ SCDs retrieved with irradiance as a reference show large biases and errors, particularly the central part of the measurement swath (Fig. 4b). Therefore, it is not optimal to use the direct sun irradiance spectra as a reference. To avoid the influence of abnormal irradiance spectra, we use cloud-free earth radiance measurements over the Pacific Ocean as a reference[21]. Compared to using solar irradiance as a reference, using earth radiance as a reference greatly reduced the spectral noise in the fit residual (Fig. 4a, b),
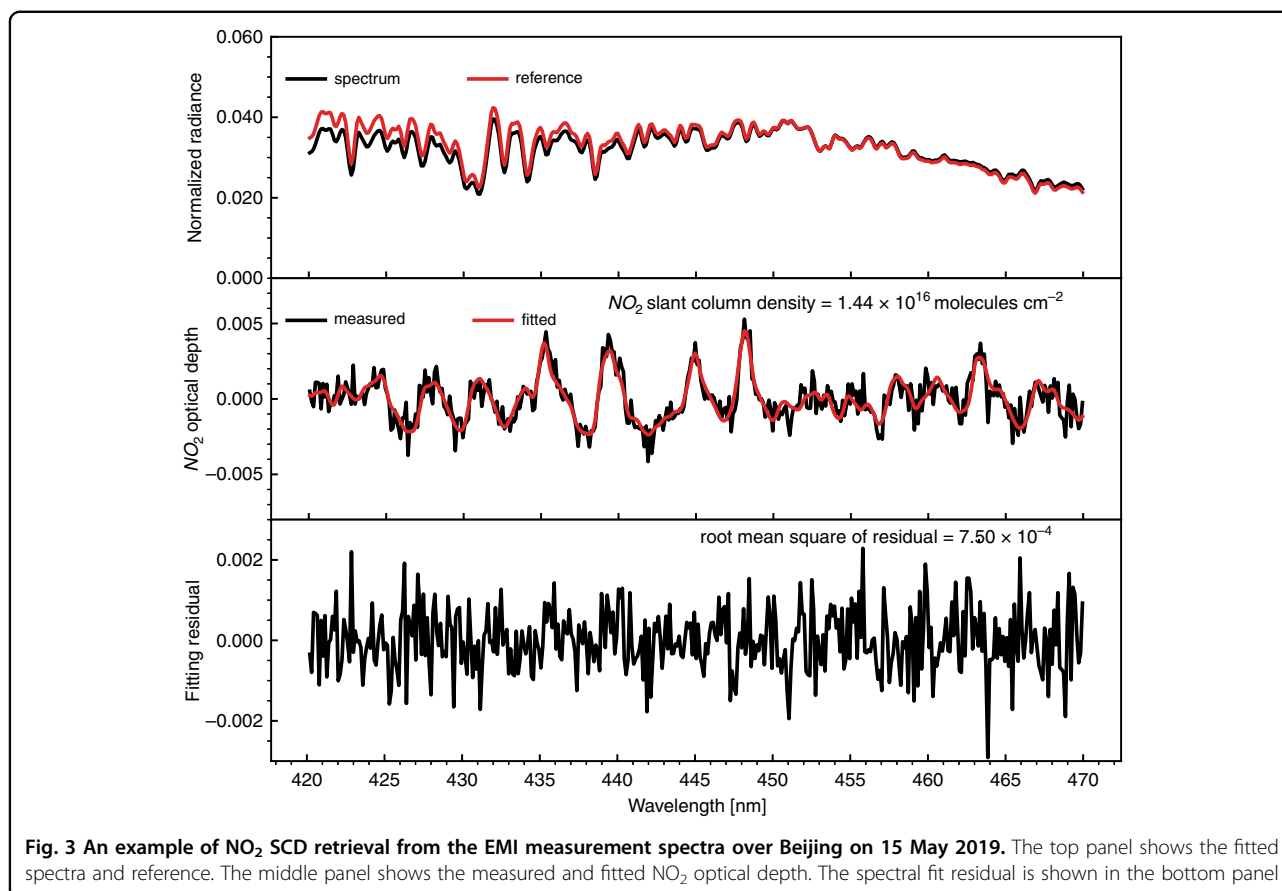
Fig. 3 An example of NO$_2$ SCD retrieval from the EMI measurement spectra over Beijing on 15 May 2019. The top panel shows the fitted spectra and reference. The middle panel shows the measured and fitted NO$_2$ optical depth. The spectral fit residual is shown in the bottom panel
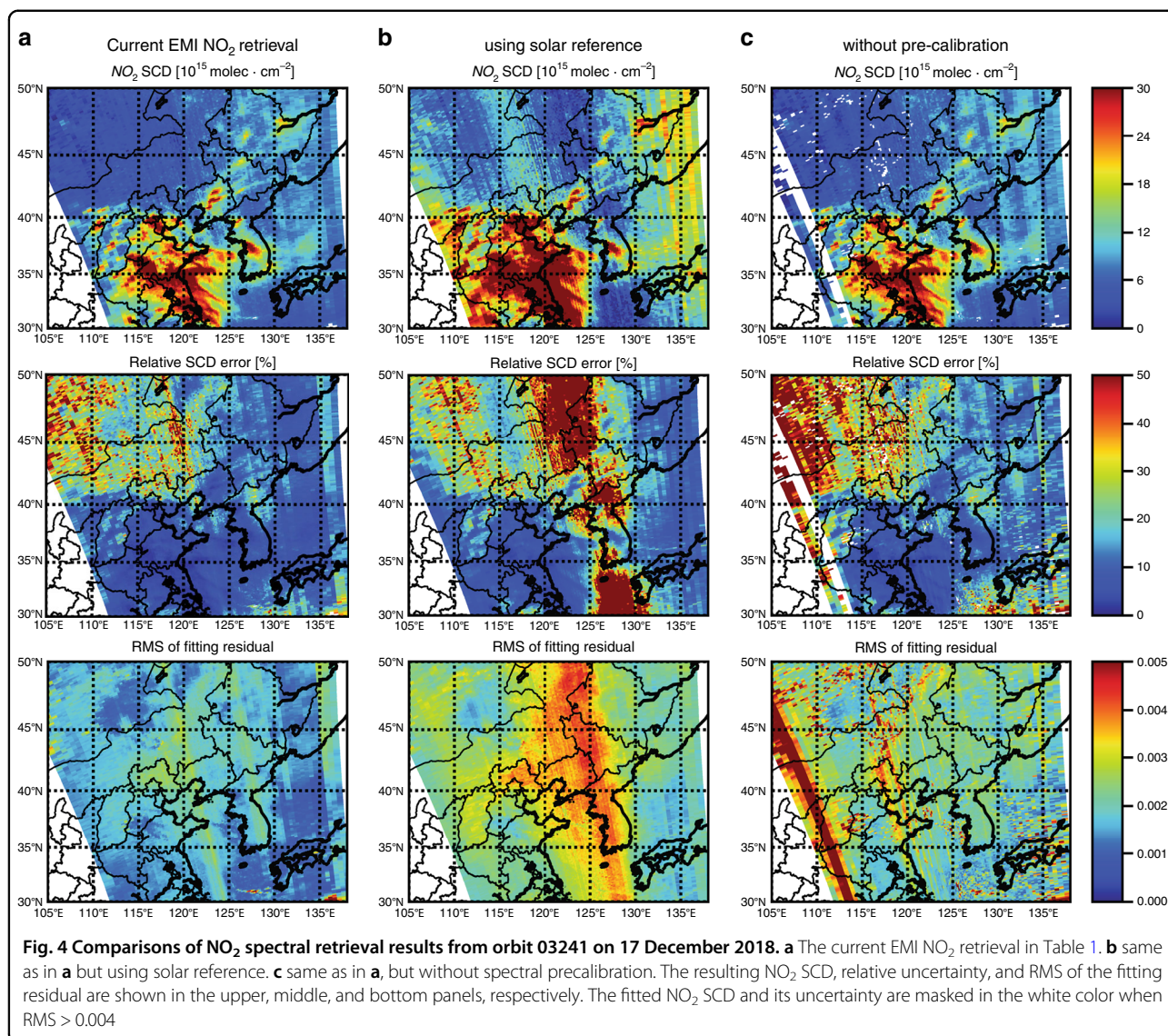
which is likely related to the differences between spectra measured with the solar and earth-viewing modes[21]. The mean RMS of fitting residual by using earth radiance as a reference over cloud-free regions is 30% smaller than that with irradiance as a reference, as shown in Fig. 4a, b.

Although using radiance as a reference improved the spectral retrieval, the radiance reference also contains a NO$_2$ absorption signal. Therefore, we must calculate the SCD offset to compensate for the residual NO$_2$ signal in the reference spectrum. The SCD offset is calculated using the NO$_2$ AMFs multiplied by the a priori NO$_2$ profile taken from the GEOS-Chem model simulations (Supplementary Fig. 2). The NO$_2$ simulation over clean remote regions is generally consistent with independent satellite observations, with a monthly mean bias of $<0.26 \times 10^{15}$ molecules cm^{-2} (Supplementary Fig. 3). Then, the SCD offset is added back to the NO$_2$ SCDs. Note that the reference spectra are selected for each cross-track row to minimize the cross-track bias due to instrument artifacts. The systematic cross-track bias in EMI NO$_2$ SCDs (the so-called "stripes", see Supplementary Fig. 4) is also observed for the OMI and TROPOMI products, and this bias can also be mitigated by using earth radiance as the reference spectrum[21].

To account for the small variation in the spectral alignment due to the thermal variation in space[12], we calibrated the additional spectral shift or squeeze and instrument slit function through cross-correlation with a high-resolution solar spectrum atlas[22] prior to the NO$_2$ DOAS fitting. The precalibrated measurement spectra lead to an ~30% smaller SCD fitting uncertainty than using initial calibration parameters (Fig. 4c), as well as a fit residual, and the SCD is nearly unchanged (within ~3.3%).
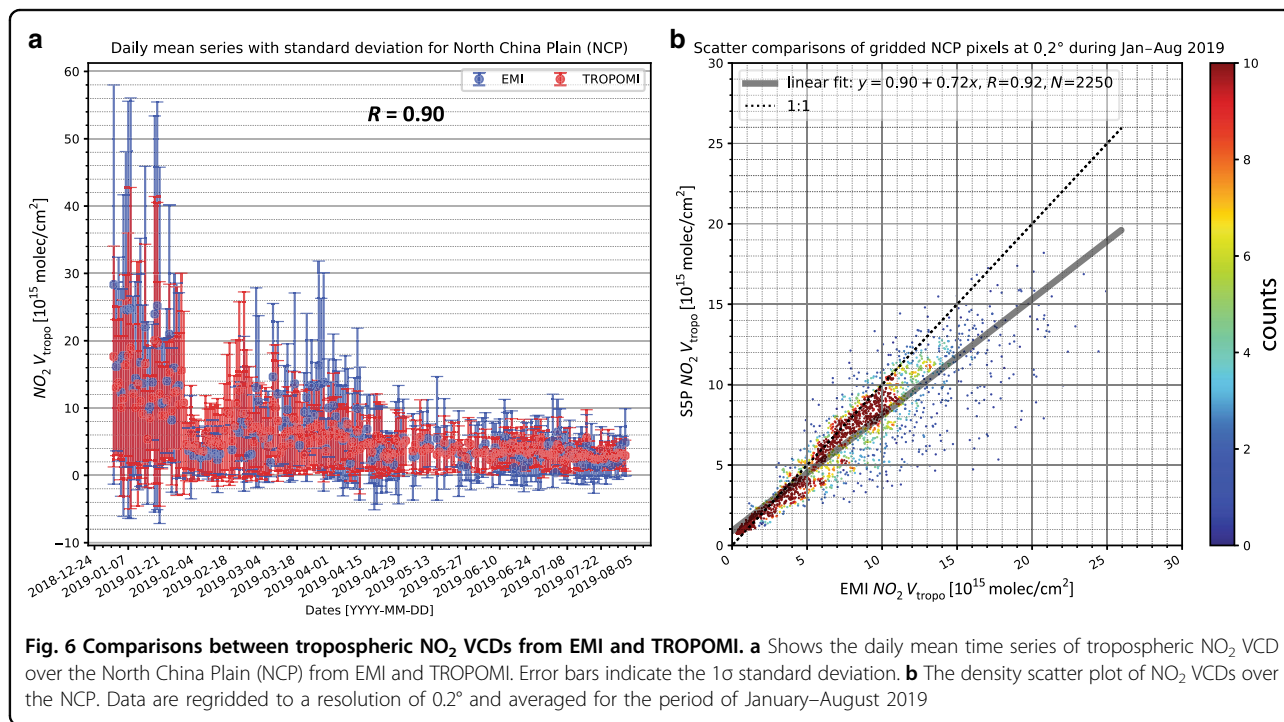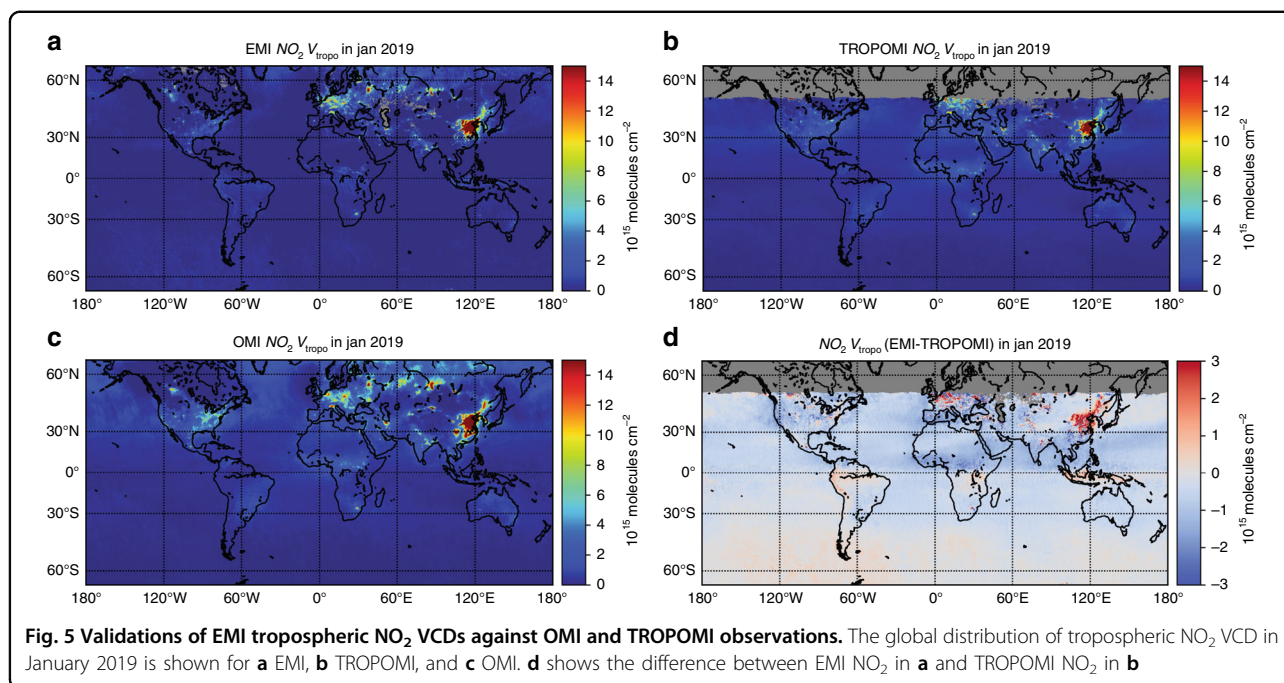
Discussion

The tropospheric NO$_2$ VCDs retrieved from EMI spectra are first validated against the OMI QA4ECV NO$_2$ products and the operational TROPOMI NO$_2$ products[23]. EMI measurements are compared to the OMI and TROPOMI products due to their similar instrument characteristics, i.e., the push-broom design, spectral bands, and near-noon overpass time at ~13:30. Note that the TROPOMI NO$_2$ product generally followed the OMI QA4ECV NO$_2$ retrieval algorithm, but TROPOMI has a higher signal-to-noise ratio and spatial resolution[23]. Figure 5 shows the monthly averaged NO$_2$ VCDs measured by EMI, OMI, and TROPOMI in January 2019. EMI NO$_2$ VCDs generally show similar spatial patterns and

Fig. 4 Comparisons of NO₂ spectral retrieval results from orbit 03241 on 17 December 2018. a The current EMI NO₂ retrieval in Table 1. **b** same as in **a** but using solar reference. **c** same as in **a**, but without spectral precalibration. The resulting NO₂ SCD, relative uncertainty, and RMS of the fitting residual are shown in the upper, middle, and bottom panels, respectively. The fitted NO₂ SCD and its uncertainty are masked in the white color when RMS > 0.004

amplitudes of NO₂ VCDs compared to OMI and TRO-POMI, while finer-scale details of NO₂ are captured by the satellite instrument with a higher spatial resolution. The EMI dataset overestimates NO₂ VCDs by up to 50% over polluted regions, such as the North China Plain (NCP) and India (Fig. 5d) compared to the TROPOMI observations. The spatiotemporal correlations between EMI NO₂ and TROPOMI NO₂ were also evaluated. For data taken from January to August 2019, the correlation coefficient (R) of daily mean NO₂ VCD time series over NCP between EMI and TROPOMI is 0.90, while the spatial correlation coefficient (R) of mean NO₂ VCDs over the NCP is 0.92 (Fig. 6). The remaining discrepancies between EMI and TROPOMI are mainly due to the NO₂ vertical profile used in the tropospheric AMF calculation, while the spectral fitting method (<3%) and stratospheric estimation method (<10%) only show a minor contribu-tion (Supplementary Fig. 5).

The EMI tropospheric NO₂ VCDs are also compared to the ground-based NO₂ measurements from the Multi-AXis Differential Optical Absorption Spectroscopy (MAX-DOAS) instruments over northern China. A good agreement with a Pearson correlation coefficient (R) of 0.82 is found between the two datasets during January–August 2019 (Fig. 7, Supplementary Fig. 6). However, EMI generally underestimates tropospheric NO₂ VCDs by 30% compared to MAX-DOAS. The biases can be explained by the difference in spatial coverage between the ground-based and satellite observations[24,25]. In general, both satellite and ground-based validations of EMI NO₂ measurements show good agreement with correlation coefficients (R) of 0.8–0.9, indicating that a

Fig. 5 Validations of EMI tropospheric NO$_2$ VCDs against OMI and TROPOMI observations. The global distribution of tropospheric NO$_2$ VCD in January 2019 is shown for **a** EMI, **b** TROPOMI, and **c** OMI. **d** shows the difference between EMI NO$_2$ in **a** and TROPOMI NO$_2$ in **b**

Fig. 6 Comparisons between tropospheric NO$_2$ VCDs from EMI and TROPOMI. a Shows the daily mean time series of tropospheric NO$_2$ VCD over the North China Plain (NCP) from EMI and TROPOMI. Error bars indicate the 1σ standard deviation. **b** The density scatter plot of NO$_2$ VCDs over the NCP. Data are regridded to a resolution of 0.2° and averaged for the period of January–August 2019

new EMI tropospheric NO$_2$ retrieval provides reliable results for the investigation of air pollution distribution.

Materials and methods

The stratosphere–troposphere separation

The stratospheric contribution of NO$_2$ must be subtracted from the total NO$_2$ column to derive the

tropospheric NO$_2$ column. In the EMI NO$_2$ retrieval, we used the STRatospheric Estimation Algorithm from Mainz[14] to estimate the stratospheric contribution, which is based on the assumption that there is negligible contribution of tropospheric NO$_2$ columns over the remote Pacific and cloudy pixels in the middle latitudes. The weighting factors based on cloud and polluted regions,
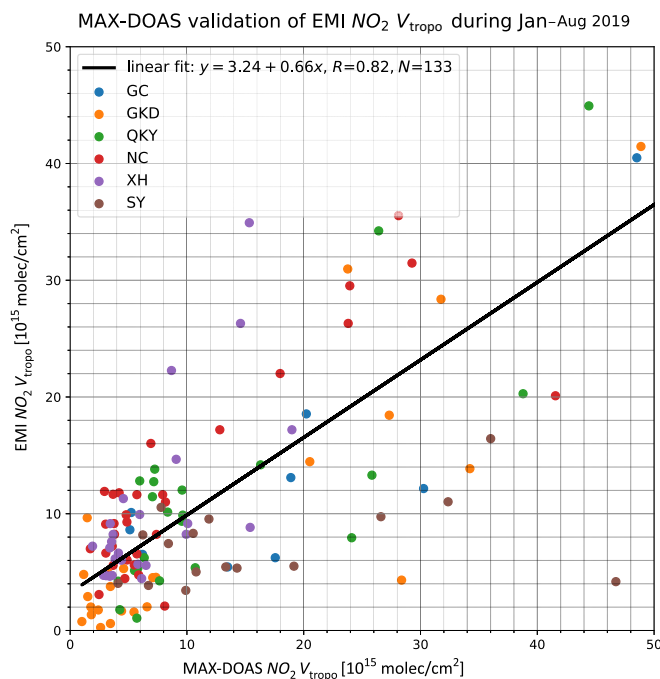
Fig. 7 Scatter plot of EMI tropospheric NO_2 VCD against ground-based MAX-DOAS observations in northern China. Measurements from six different measurement sites are used in the comparison: the Gucheng site (GC, 39.149°N, 115.734°E) in the Hebei Province, the Guokeda site (GKD, 40.408°N, 116.675°E) in Beijing, the Qikeyuan (QKY, 39.9472°N, 116.3206°E) site in Beijing, the Nancheng (NC, 39.781°N, 116.127°E) site in Beijing, the Xianghe site (XH, 39.750°N, 116.095°E) in the Hebei Province, and the Shengyang site (SY, 41.812°N, 123.401°E) in the Liaoning Province

which determines their impacts on the stratospheric estimate, are assigned to each satellite pixel. Subsequently, spatial smoothing based on weighted convolution is used to estimate the global stratospheric column.

NO_2 AMF calculations

The EMI NO_2 AMFs of each atmospheric layer (i.e., Box-AMFs) are calculated at 445 nm by the linearized pseudospherical vector model VLIDORT[26] version 2.7. In addition to the solar and satellite-viewing geometries provided in the level 1 data, additional atmospheric and surface information are needed in the AMF calculations. Surface albedo at 442 nm is taken from the OMI minimum earth's surface Lambertian equivalent reflectance[27] and interpolated to the EMI footprints. Considering the same local overpass time between EMI and TROPOMI, cloud top pressure and cloud fraction from TROPOMI[28] are used for the calculations of EMI NO_2 AMFs. A priori NO_2 profiles are taken from the high-resolution (~20 km) WRF-Chem simulations for the China domain and from GEOS-Chem simulations at the resolution of $2 \times 2.5°$ for the global domain (Supplementary Fig. 7). The spatial resolution of the NO_2 a priori profile is reportedly one of the dominant uncertainty sources during the NO_2 AMF calculations[29]. To expedite the calculation, these box-AMFs are precalculated and stored in the six-dimensional lookup table. Then, the box-AMF for each EMI

observation can be derived by interpolating within the lookup table.

Author details
[1]School of Earth and Space Sciences, University of Science and Technology of China, Hefei 230026, China. [2]Department of Precision Machinery and Precision Instrumentation, University of Science and Technology of China, Hefei 230026, China. [3]Key Laboratory of Environmental Optics and Technology, Anhui Institute of Optics and Fine Mechanics, Chinese Academy of Sciences, Hefei 230031, China. [4]Center for Excellence in Regional Atmospheric Environment, Institute of Urban Environment, Chinese Academy of Sciences, Xiamen 361021, China. [5]Key Laboratory of Precision Scientific Instrumentation of Anhui Higher Education Institutes, University of Science and Technology of China, Hefei 230026, China. [6]Remote Sensing Technology Institute (IMF), German Aerospace Center (DLR), Oberpfaffenhofen, Germany

Author contributions
C.Z. performed the data analysis and wrote the manuscript. C.L. supervised this research and conceived the idea. K.L.C. contributed to the data interpretation and manuscript revisions. H.L., B.L., C.X., and W.T. processed the MAX-DOAS data. H.Z., F.S., and J.L. built the EMI instrument. C.Z. prepared the paper with inputs from all co-authors.

Data availability

Conflict of interest

The authors declare that they have no conflict of interest.

References

1. Zhang, C. X. et al. Preflight evaluation of the performance of the chinese environmental trace gas monitoring instrument (EMI) by spectral analyses of nitrogen dioxide. *IEEE Trans. Geosci. Remote Sens.* **56**, 3323–3332 (2018).
2. Levelt, P. F. et al. The ozone monitoring instrument. *IEEE Trans. Geosci. Remote Sens.* **44**, 1093–1101 (2006).
3. Veefkind, J. P. et al. TROPOMI on the ESA Sentinel-5 Precursor: a GMES mission for global observations of the atmospheric composition for climate, air quality and ozone layer applications. *Remote Sens. Environ.* **120**, 70–83 (2012).
4. Atkinson, R. Atmospheric chemistry of VOCs and NO_x. *Atmos. Environ.* **34**, 2063–2101 (2000).
5. Liu, F. et al. Recent reduction in NO_x emissions over China: synthesis of satellite observations and emission inventories. *Environ. Res. Lett.* **11**, 114002 (2016).
6. Crippa, M. et al. Gridded emissions of air pollutants for the period 1970-2012 within EDGAR v4.3.2. *Earth Syst. Sci. Data* **10**, 1987–2013 (2018).
7. An, Z. S. et al. Severe haze in northern China: a synergy of anthropogenic emissions and atmospheric processes. *Proc. Natl Acad. Sci. USA* **116**, 8657–8666 (2019).
8. Gao, M. et al. Estimates of health impacts and radiative forcing in winter haze in eastern china through constraints of surface $PM_{2.5}$ predictions. *Environ. Sci. Technol.* **51**, 2178–2185 (2017).
9. Liu, F. et al. NO_x emission trends over Chinese cities estimated from OMI observations during 2005 to 2015. *Atmos. Chem. Phys.* **17**, 9261–9275 (2017).
10. Zhang, C. X. et al. Satellite UV-Vis spectroscopy: implications for air quality trends and their driving forces in China during 2005-2017. *Light. Sci. Appl.* **8**, 100 (2019).
11. Liu, X. L. et al. Assimilation of satellite NO_2 observations at high spatial resolution using OSSEs. *Atmos. Chem. Phys.* **17**, 7067–7081 (2017).
12. Zhao, M. J. et al. Preflight calibration of the Chinese Environmental trace gases monitoring instrument (EMI). *Atmos. Meas. Tech.* **11**, 5403–5419 (2018).
13. Platt, U. & Stutz, J. *Differential Optical Absorption Spectroscopy*, pp 135–174 (Springer, Berlin, Heidelberg, 2008).
14. Beirle, S. et al. The STRatospheric Estimation Algorithm from Mainz (STREAM): estimating stratospheric NO_2 from nadir-viewing satellites by weighted convolution. *Atmos. Meas. Tech.* **9**, 2753–2779 (2016).
15. Valks, P. et al. Operational total and tropospheric NO_2 column retrieval for GOME-2. *Atmos. Meas. Tech.* **4**, 1491–1514 (2011).
16. Palmer, P. I. et al. Air mass factor formulation for spectroscopic measurements from satellites: application to formaldehyde retrievals from the global ozone monitoring experiment. *J. Geophys. Res.* **106**, 14539–14550 (2001).
17. Boersma, K. F. et al. Improving algorithms and uncertainty estimates for satellite NO_2 retrievals: results from the quality assurance for the essential climate variables (QA4ECV) project. *Atmos. Meas. Tech.* **11**, 6651–6678 (2018).
18. Zhao, M. J. et al. Effect of AO/UV/RD exposure on spaceborne diffusers: a comparative experiment. *Appl. Opt.* **54**, 9157–9166 (2015).
19. Schenkeveld, V. M. E. et al. In-flight performance of the ozone monitoring instrument. *Atmos. Meas. Tech.* **10**, 1957–1986 (2017).
20. Heath, D. F. et al. The solar backscatter ultraviolet and total ozone mapping spectrometer (SBUV/TOMS) for Nimbus G. *Optical Eng.* **14**, 144323 (1975).
21. Anand, J. S., Monks, P. S. & Leigh, R. J. An improved retrieval of tropospheric NO_2 from space over polluted regions using an Earth radiance reference. *Atmos. Meas. Tech.* **8**, 1519–1535 (2015).
22. Chance, K. & Kurucz, R. L. An improved high-resolution solar reference spectrum for earth's atmosphere measurements in the ultraviolet, visible, and near infrared. *J. Quant. Spectrosc. Radiat. Transf.* **111**, 1289–1295 (2010).
23. Griffin, D. et al. High-resolution mapping of nitrogen dioxide with TROPOMI: first results and validation over the canadian oil sands. *Geophys. Res. Lett.* **46**, 1049–1060 (2019).
24. Chan, K. L. et al. Observations of tropospheric aerosols and NO_2 in Hong Kong over 5 years using ground based MAX-DOAS. *Sci. Total Environ.* **619-620**, 1545–1556 (2018).
25. Chan, K. L. et al. MAX-DOAS measurements of tropospheric NO_2 and HCHO in Nanjing and a comparison to ozone monitoring instrument observations. *Atmos. Chem. Phys.* **19**, 10051–10071 (2019).
26. Spurr, R. J. D. VLIDORT: a linearized pseudo-spherical vector discrete ordinate radiative transfer code for forward model and retrieval studies in multilayer multiple scattering media. *J. Quant. Spectrosc. Radiat. Transf.* **102**, 316–342 (2006).
27. Kleipool, Q. L. et al. Earth surface reflectance climatology from 3 years of OMI data. *J. Geophys. Res.* **113**, D18308 (2008).
28. Loyola, D. G. et al. The operational cloud retrieval algorithms from TROPOMI on board Sentinel-5 Precursor. *Atmos. Meas. Tech.* **11**, 409–427 (2018).
29. Kuhlmann, G. et al. Development of a custom OMI NO_2 data product for evaluating biases in a regional chemistry transport model. *Atmos. Chem. Phys.* **15**, 5627–5644 (2015).
30. van den Oord, G. H. J. et al. OMI level 0 to 1b processing and operational aspects. *IEEE Trans. Geosci. Remote Sens.* **44**, 1380–1397 (2006).
31. Dirksen, R. et al. Prelaunch characterization of the Ozone Monitoring Instrument transfer function in the spectral domain. *Appl. Opt.* **45**, 3972–3981 (2006).
32. Williams, J. E. et al. The high-resolution version of TM5-MP for optimized satellite retrievals: description and validation. *Geosci. Model Dev.* **10**, 721–750 (2017).
33. Wang, S. W. et al. Growth in NO_x emissions from power plants in China: bottom-up estimates and satellite observations. *Atmos. Chem. Phys.* **12**, 4429–4447 (2012).
34. Su, W. J. et al. Characterization of ozone in the lower troposphere during the 2016 G20 conference in Hangzhou. *Sci. Rep.* **7**, 17368 (2017).